



Electrochemical sensor based on multi-walled nanotubes for investigating the damage and action of 6-mercaptopurine on double-stranded DNA

Received 00th January 20xx,
Accepted 00th January 20xx

DOI: 10.1039/x0xx00000x

www.rsc.org/

Wenwei Tang^{a#*}, Weihao Li^{b#}, Min Zhang^c, Xinpeng Zeng^{c*}

Abstract: Biosensors based on nanomaterials provide a means for sensitive and rapid detection of DNA damage. To investigate the electrochemical behavior of 6-mercaptopurine (6-MP), including the damage to double-stranded deoxyribonucleic acid (dsDNA) by 6-MP and its damage mechanisms, a dsDNA/MWNTs/CTS/GCE biosensor was constructed using of multi-walled carbon nanotubes (MWNTs) and chitosan (CTS) as the modified materials. The experimental results showed that after modified, the active area of the MWNTs/CTS/GCE significantly increased and the oxidation peak current of the MWNTs/CTS/GCE in response to $K_3[Fe(CN)_6]$ exhibited a remarkable increase. The characteristic peak of 6-MP on the biosensor was determined to be approximately 0.55 V using differential pulse voltammetry (DPV). Clear damage to dsDNA caused by 6-MP was observed. The damage to adenine was more severe than to guanine. The interaction between 6-MP and dsDNA could be explained as an intercalation during the electrochemical oxidation process on the modified electrode, which was an irreversible process controlled by adsorption and was accompanied by the transfer of a single electron coupled with a single proton.

Keywords: biosensor; multi-walled carbon nanotubes; 6-mercaptopurine; intercalation; DNA damage

1. Introduction

Anti-cancer drugs can interact with DNA and affect DNA replication. Therefore, DNA is the main molecule targeted by the action of some anti-cancer drugs. Studies on the interactions between anti-cancer drugs and DNA constitute the basis for understanding the DNA breakage reaction. Studies on these interactions are of great significance not only for demonstrating the effectiveness of anti-cancer drugs and carcinogenesis mechanisms but also for designing synthetic anti-cancer drugs that target DNA¹⁻⁴. In general, small molecules (including anti-cancer drugs) primarily interact with DNA through non-covalent binding, which is divided into groove binding, electrostatic binding and intercalated combination. Shen et al.⁵ discovered that DNA decreased the reduction peak current for melamine, leading to a slight negative shift in the peak potential. They reported that melamine potentially combined with DNA through groove binding. Wang et al.⁶ reported that the presence of DNA led to a decrease in the peak current of nicotine and a negative shift in the potential, indicating that nicotine could interact with

DNA through electrostatic binding. Li et al.⁷ observed that the interaction of mitoxantrone (MTX) with DNA could result in a significant decrease in the peak current of MTX and a bathochromic shift in the peak potential. They confirmed that MTX interacted with DNA through the intercalative mode, and furthermore, only a portion of the chromophore of MTX, including rings A and B, was involved in the intercalation into DNA base pairs.

Many methods and techniques have been used for detecting DNA damage and the interaction between DNA and anti-cancer drugs, such as mass spectrometry⁸, fluorescence⁹, chromatography¹⁰ and capillary electrophoresis¹¹. Because electron transfers with DNA as a medium are essential for many processes, such as interfering with genetic information transfer, inducing misreading of genetic information, damaging DNA and mutating cells¹²⁻¹⁵, by monitoring the changes in voltage or current through the electrode surface¹⁶⁻²⁰, the electrochemical method can provide rapid evaluations and valid predictions of DNA damage and of the interactions between DNA and anti-cancer drugs. Electrochemical sensors can overcome the limitations associated with the traditional detection techniques⁸⁻¹¹ because of less complicated pretreatments, less expensive instruments and shorter analysis times.

Although DNA molecules possess electroactive purine bases such as guanine and adenine, the electrochemical responses of these base residues are usually too weak to be detected using conventional electrodes. To overcome this problem,

Department of Chemistry, Tongji University, Shanghai, 200092, China
Handan municipal centre for disease control and prevention, Handan,
056000, China

School of Life Science and Technology, Tongji University, Shanghai, 200092, China

[#]These authors contributed equally to this work.

*Corresponding author

E-mail: tangww@tongji.edu.cn; zengxp@tongji.edu.cn

researchers have been exploring the use of suitable modified materials. Because nanomaterials can accelerate electron transfer, increase the probe adsorption capacity on the electrode surface and reinforce and amplify the electrical signal of the marker, electrodes modified with nanomaterials can accurately detect changes in the electrochemical signals. Carbon nanotubes, which are one type of nanomaterial, have attracted considerable attention. These nanotubes are divided into multi-walled carbon nanotubes (MWNTs) and single-walled carbon nanotubes (SWNTs). MWNTs consist of multiple rolled layers (concentric tubes) of carbon atoms (a single hexagonal carbon layer). They have a small particle size, large specific surface area, high surface reactivity, and high catalytic efficiency. MWNTs are compatible with many other compositions. A DNA/MWNTs/GCE electrode modified with MWNTs dispersed in Nafion was capable of providing a sensitive voltammetric response for monitoring phenolic pollutants²¹. The modification of a glassy carbon electrode (GCE) with MWNTs, quercetin and a PFSA/PTEE polymer was successfully used for the electrochemical determination of dopamine²². Wu used SWNTs and ferriporphyrin to modify a GCE, which was then applied to measure Susan I with a linear range varying from 5.03×10^{-8} to 2.01×10^{-6} M and a detection limit of 1×10^{-8} M²³. Moreover, materials with good electrical conductivity and biocompatibility are required to cross-link the nanomaterials and the electrode to create sensors. Chitosan (CTS) is an environmentally friendly, natural polymer. This molecule contains a large number of hydroxyl and amino groups. The amino groups are not only conducive to covalent bonding with enzymes and proteins but also to chelating metal ions. A Nafion/carbon-coated iron nanoparticle-chitosan composite film was used to modify a GCE, and the obtained GCE was highly selective for dopamine²⁴.

6-Mercaptopurine (6-MP) is an antimetabolite that exerts immunosuppressive action by suppressing the metabolism of purine and thereby disturbing the synthesis of nucleic acids. 6-MP is an ideal anti-cancer drug for clinical therapy, and it is generally used to treat acute leukemia and chorionic epithelioma, among others^{25, 26}. Early electrochemical studies on 6-MP were generally performed using the polarographic method in a dilute acid medium²⁷. The ion-selective electrode method was also used in studies on 6-MP²⁸. These studies primarily focused on the working conditions (selection of supporting electrolyte, choice of electrode, electrolyte acidity regulator and so on), however, the studies on the electrode reaction mechanism were not sufficient. The aforementioned studies did not provide convincing data for studies on drug testing, drug metabolism, and pharmacology.

In this work, 6-MP was adopted as the study target, and a dsDNA/MWNTs/CTS/GCE was developed using MWNTs and CTS as the composite materials to modify the electrode. The electrochemical behavior of 6-MP on the dsDNA/MWNTs/CTS/GCE was explored using cyclic voltammetry (CV), electrochemical impedance spectroscopy (EIS), differential pulse voltammetry (DPV) and other methods, and damage to dsDNA by 6-MP and its mechanisms were studied. The research results could provide a valuable method

to construct biosensors for detecting anti-cancer drugs, which would have widely applications in the fields of medicine and life sciences.

2. Experimental

2.1 Reagents and materials

Glassy carbon electrodes (GCE, GC130, Φ 3 mm) were purchased from Tianjin Aidahengsheng Technology Co., Ltd., China. The multi-walled carbon nanotubes (MWNTs, > 95% purity) were purchased from the Chengdu Organic Chemicals Co., Ltd., China. The reagents used in this study, such as chitosan, potassium ferricyanide, glacial acetic acid, 6-MP and sodium acetate, were of analytical grade and were purchased from the Sinopharm Chemical Reagent Co., Ltd., China. The biochemical pure herring sperm double-stranded DNA was purchased from Sigma, United States.

2.2 Functional modification and synthesis of MWNTs

MWNTs were added to concentrated nitric acid under vigorous stirring prior to sonication for 1 h. After washing with distilled water to neutral pH, MWNTs were dried in a 37 °C incubator. 10 mg pretreated MWNTs were added to 10 mL 0.2% (m/v) aqueous solution of sodium dodecyl sulfonate and sonicated for 1 h. The resulting MWNTs solution was stored at 4 °C for future use.

2.3 Pretreatment of the glassy carbon electrode

The electrode was polished in a 'figure 8' pattern using alumina powders with diameters of 0.3, 0.1 and 0.05 μ m. The electrode was then successively dipped into distilled water, ethanol and distilled water to perform ultrasonic cleaning. The pretreated GCE was placed in an 80-mL solution composed of 0.2 M KCl and 5 mM $K_3[Fe(CN)_6]$, and a CV test was performed. After the CV results met the standard ($\Delta E_p < 80$ mV), the GCE was washed again with distilled water and stored for use.

2.4 Preparation of the modified electrode

CTS/GCE: 70 mg of CTS was added to 10 mL of a 1 wt% acetic acid solution. The mixed solution was then ultrasonicated, which resulted in a 0.7% (w/v) mixed solution of CTS and acetic acid. A 10 μ L aliquot of the mixed solution was used to evenly coat the GCE. Finally, the coated GCE was dried at room temperature.

MWNTs/CTS/GCE: 1 mg of MWNTs was added to 2 mL of a 0.7% (w/v) mixed solution of CTS and acetic acid. The mixed solution was ultrasonicated, which afforded a 0.5 mg/mL MWNTs/CTS dispersion. Similarly, a 10 μ L aliquot of the dispersion was used to evenly coat the GCE, and the coated GCE was dried at room temperature.

dsDNA/MWNTs/CTS/GCE: 9 mg of herring sperm double-stranded DNA was dissolved in 1 mL of a tris-HCl solution, which afforded a 9 mg/L dsDNA solution. The dsDNA solution was then coated on the surface of the MWNTs/CTS/GCE, and the coated GCE was stored in a 4 °C refrigerator.

2.5 Raman analysis

Raman spectra can provide molecular vibration and rotation information for studying molecular structures. A Renishaw

inVia Raman spectrometer was used to characterize the samples in this study. For this instrument, the light passing efficiency is greater than 30%, the spectral resolution is 1 cm^{-1} , the optical maser wavelength is 254 nm, and the tested Raman shift is between 100 and 3200 cm^{-1} .

2.6 Electrochemical test

The electrochemical behavior of the electrode was investigated using an Autolab model PGSTAT30 electrochemical workstation. For the tests, the prepared electrode, a platinum electrode and a saturated calomel electrode were used as the working electrode, the counter electrode and the reference electrode, respectively. During the CV tests, the scan speed was 50 mV/s , and the scan range was from -0.1 to 0.6 V . The frequency range of the EIS test was $10000\text{--}0.1\text{ Hz}$, and the electric potential amplitude was 50 mV . The modulation amplitude during the DPV tests was 0.05 V , the waiting electric potential was 0 V , the interval time was 0.2 s , and the pulse time was 0.05 s . For the CC measurements, the equilibrium time was 2 s , the interval time was 0.1 s , and the potential duration was 0.25 V/s .

3. Results and discussion

3.1 Raman spectrum of MWNTs

Raman scattering is a powerful method for studying MWNTs and plays an important role in understanding the physical structure of MWNTs. The Raman spectrum was measured with the basic Raman-active mode of the MWNTs as shown in Fig. 1. A strong peak can be observed at approximately 1580 cm^{-1} , which corresponds to the 'G' peak of the MWNTs. Originating from the first-order vibration of the E_{2g} phonon planar motion, this 'G' peak can serve as the indicator of the degree of symmetry and the order of the materials. A relatively weak peak can be observed in the range from 1250 to 1450 cm^{-1} , which corresponds to the D-mode in graphene. The intensity ratio between the G-mode and D-mode can be used to describe the amount of point defects in the graphite structure, and it reflects the degree of sample impurity and disorder.

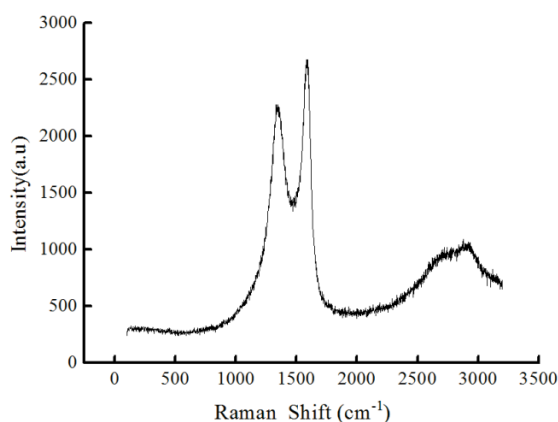


Fig. 1. Raman spectrum of MWNTs.

3.2 Characterization of the GCEs with different modifications

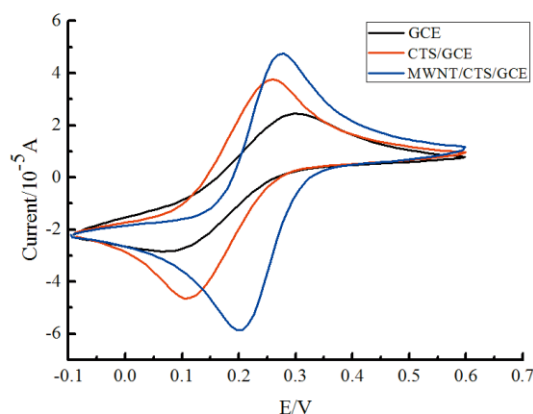


Fig. 2. The CV curves of different modified electrodes in a 0.2 M KCl solution containing $5 \times 10^{-3}\text{ M K}_3[\text{Fe}(\text{CN})_6]$.

As shown in Fig. 2, redox peaks with favorable reversibility appeared for both non-modified and modified electrodes. In contrast with GCE, after modification with CTS, the redox current of CTS/GCE increased slightly, primarily because a larger amount of $[\text{Fe}(\text{CN})_6]^{3-}$ was adsorbed by the CTS/GCE through electrostatic attractions by the positively charged amino groups in CTS.

Compared with GCE and CTS/GCE, the redox current of MWNTs/CTS/GCE clearly increased. On the one hand, the specific surface area of the electrode increased after the modification with the MWNTs, which resulted in an increase in the amount of $[\text{Fe}(\text{CN})_6]^{3-}$ adsorbed on the electrode surface. On the other hand, the MWNTs functioned as a molecular wire characterized by high conductivity. Compared with the bare GCE, the redox current of the MWNTs/CTS/GCE increased from 0.02 mA to 0.05 mA , suggesting that the GCE modified by CTS and MWNTs exhibited high sensitivity to the electrochemical signals.

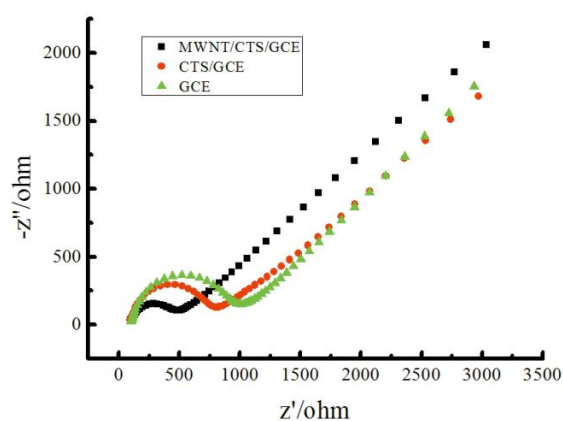


Fig. 3. The EIS curves of different modified electrodes in a 0.1 M KCl solution containing $5 \times 10^{-3}\text{ M K}_3[\text{Fe}(\text{CN})_6]/\text{K}_4[\text{Fe}(\text{CN})_6]$.

Fig. 3 shows that all three electrodes exhibited regular semi-arc curves in the high-frequency region, and from GCE to MWNTs/CTS/GCE, the radius of the semi-arc gradually

decreased. According to Nyquist's Theorem, the smaller the radius of the semi-arc is, the smaller is the impedance value of the modified electrode surface. Compared with the original GCE, the impedance value of CTS/GCE was smaller because the amino groups in CTS were beneficial to the combination with the anions in the solution, promoting charge transfer. Likewise, the impedance value of MWNTs/CTS/GCE was the smallest because MWNTs have excellent electrical conductivity and outstanding size and surface effects.

3.3 Effect of MWNTs modified concentration on electrode

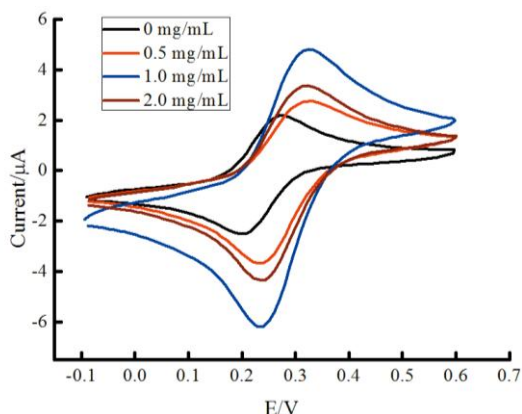


Fig. 4. The CV curves of the electrodes modified with different concentrations of MWNTs in a 0.2 M KCl solution containing 5×10^{-3} M $K_3[Fe(CN)_6]$.

The electrodes were coated with different amounts of MWNTs, and the CV results are shown in Fig. 4. The performance of the modified electrodes was significantly improved with the coating amounts from 0 to 1 mg/mL, and the potential difference of the redox peak decreased gradually. However, the redox peak current clearly decreased as the coating amount increased to 2 mg/mL. One potential reason for this result is that as the concentration of MWNTs increased, the thickness of the modified layer on the electrode increased, which caused the distance from the charge to the electrode surface to increase, thereby lowering the conductivity of the electrode.

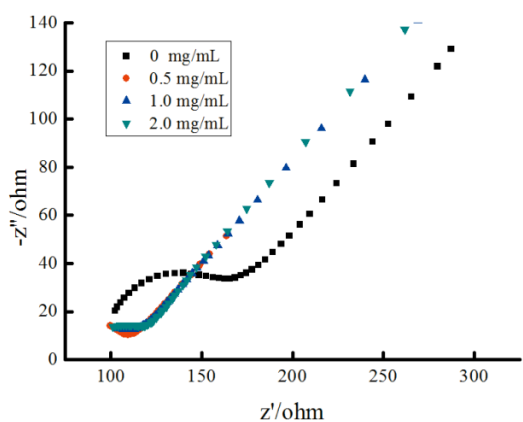


Fig. 5. The EIS curves of the electrodes modified with different concentrations of MWNTs in a 0.1 M KCl solution containing 5×10^{-3} M $K_3[Fe(CN)_6]/K_4[Fe(CN)_6]$.

As shown in Fig. 5, in the high-frequency region, GCE exhibited a larger semi-arc radius, whereas the modified electrode with the coating amounts from 0 to 2 mg/mL exhibited a relatively smaller semi-arc radius, implying that the use of MWNTs could result in a significant reduction in the impedance of the electrode surface. As in the case above, the semi-arc radius increased as the coating amount increased to 2 mg/mL.

To perform a comprehensive analysis using CV and EIS, the optimal concentration of MWNTs for modifying the electrode was selected to be 1 mg/mL.

3.4 Activation area of the modified electrodes

The electrochemical activity of a working electrode is closely related to its active surface area. With 1×10^{-4} M $K_3[Fe(CN)_6]$ as the model compound, the active area of the electrode modified with the compound materials was calculated using chronocoulometry.

The analyses were conducted according to the chronocoulometry formula:

$$Q_d = \frac{2nFAD_0^{1/2}C_0t^{1/2}}{\pi^{1/2}} + Q_{dl} + nFA\Gamma_0 \quad (1)$$

where Q_d is the charge (C); n is the number of electrons transferred during the electrode reaction; F is Faraday's constant; A is the active surface area of the electrode (cm^2); D_0 is the diffusion coefficient of 1×10^{-4} M $K_3[Fe(CN)_6]$ in the 1 M KCl supporting electrolyte, which is $7.6 \times 10^{-6} \text{ cm}^2 \text{ s}^{-1}$ ²⁹; t is the electrolysis time (s); C_0 is the initial molar concentration (M) of the active substance in solution; Q_{dl} is the double layer charge, which can be eliminated by subtracting the background (C); and $nFA\Gamma_0$ is the Faradaic charge (C).

According to the above formula, a linear relationship exists between Q_d and $t^{1/2}$. $Q_{dl} + nFA\Gamma_0$ is the intercept of the obtained linear equation $Q \sim t^{1/2}$.

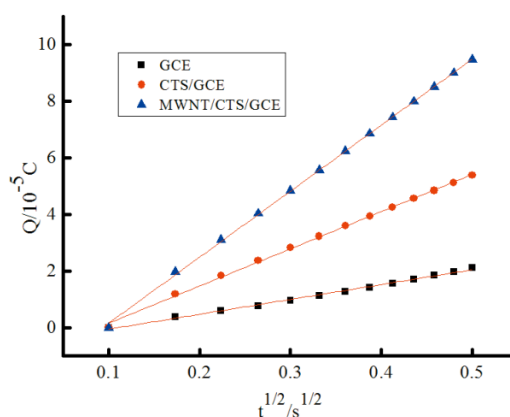


Fig. 6. The $Q \sim t^{1/2}$ curves of different modified electrodes in a 1 M KCl solution containing 1×10^{-4} M $K_3[Fe(CN)_6]$.

The relationships between Q_d and $t^{1/2}$ for the different modified electrodes in the KCl solution are shown in Fig. 6. The linear equations for GCE, CTS/GCE and MWNTs/CTS/GCE in Fig. 6 were obtained from the following linear fits:

$$y = 5.3 \times 10^{-5}x - 6.3 \times 10^{-6}, (R^2 = 0.9959) \quad (2)$$

$$y = 1.3 \times 10^{-4}x - 1.0 \times 10^{-5}, (R^2 = 0.9986) \quad (3)$$

$$y = 2.3 \times 10^{-4}x - 2.0 \times 10^{-5}, (R^2 = 0.9995) \quad (4)$$

Based on the above linear equations, the active areas of the electrodes were calculated in combination with Eq. (1). The calculated active areas of GCE, CTS/GCE and MWNTs/CTS/GCE were 1.76, 4.32 and 7.64 cm², respectively. Overall, after modification by MWNTs and CTS, the specific surface area of the electrode significantly increased. The number of effective adsorption sites on the electrode surface also increased as the specific surface area increased. When used to study the electrochemical behavior of 6-MP, these modified electrodes could enhance the adsorption capacity of the electrode to 6-MP, increase the electrical conductivity and improve the detection sensitivity.

3.5 Response of dsDNA on different modified electrodes

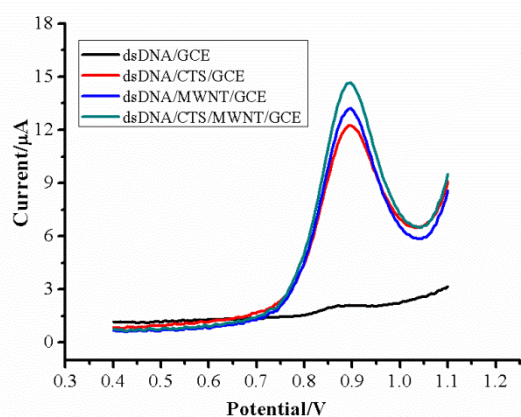


Fig. 7. The DPV curves of dsDNA on different modified electrodes in phosphate buffer (pH 5.0, 0.1 M).

The oxidation peak for guanine in dsDNA is located at approximately 0.90 V^{30,31}. As shown in Fig. 7, a fairly weak oxidation peak appeared in dsDNA/GCE at approximately 0.90 V. However, after modification with CTS and MWNTs respectively, an obvious characteristic peak located at approximately 0.90 V was observed. Due to the favorable biocompatibility of CTS, a greater amount of dsDNA was immobilized on the CTS/GCE, therefore, the oxidation peak current of dsDNA on dsDNA/CTS/GCE was larger than that on dsDNA/GCE. The large number of amino groups in CTS could also improve the charge-transfer capability of the electrode; When the GCE surface was modified with MWNTs, the oxidation peak current of guanine was increased, and higher than that of CTS-modified electrode; After further modification on CTS/GCE with MWNTs, the characteristic peak current of dsDNA significantly increased due to the excellent conductivity of MWNTs and due to the large specific surface area of MWNTs, which would improve the adsorption of dsDNA on the electrode.

3.6 Damage of dsDNA by 6-MP

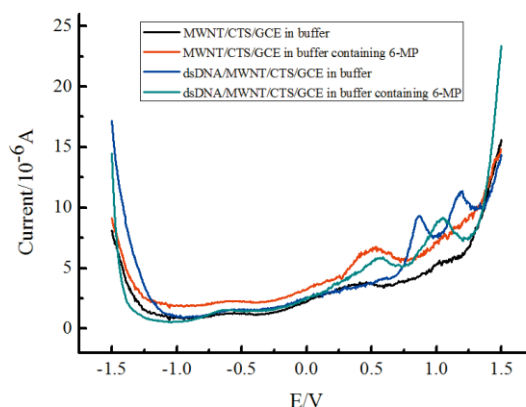


Fig. 8. The DPV curves of MWNTs/CTS/GCE and dsDNA/MWNTs/CTS/GCE in phosphate buffer (pH 5.0, 0.1 M) and phosphate buffer (pH 5.0, 0.1 M) containing 7.5×10^{-4} M 6-MP, respectively.

As shown in Fig. 8, the DPV of MWNTs/CTS/GCE in the buffer solution was flat overall, with no obvious oxidation peak. When the MWNTs/CTS/GCE was scanned in the buffer solution containing 6-MP, an oxidation peak appeared at approximately 0.55 V. By comparing the DPV curves of above, we concluded that the oxidation peak located at approximately 0.55 V was the characteristic oxidation peak for 6-MP.

After modification by dsDNA, in phosphate buffer solution, dsDNA/MWNTs/CTS/GCE exhibited two oxidation peaks located at approximately 0.9 and 1.2 V, which corresponded to the characteristic oxidation peaks of guanine and adenine in dsDNA^{30,31}. When scanned in the buffer solution containing 7.5×10^{-4} M 6-MP, two oxidation peaks appeared. The peak at approximately 0.6 V was identified as the oxidation peak for 6-MP, and the other peak at approximately 1.1 V was considered to be the oxidation peak for guanine in dsDNA^{30,31}.

Comparing the peak position and peak value of 6-MP on dsDNA/MWNTs/CTS/GCE and MWNTs/CTS/GCE in the buffer solution containing 6-MP, the oxidation peaks of 6-MP shifted toward the right, and its current peak value decreased. According to Ref.³², when small molecules interact with dsDNA, if the oxidation peak potential moves toward the right, the mode of action between the small molecules and dsDNA is intercalation. The reason for the current reduction was that dsDNA as a biomacromolecule exhibited a weaker capability for electron transfer compared with the MWNTs and CTS compound, and consequently, the charge-transfer capability of the electrode became weaker, leading to a decreased current peak value on dsDNA/MWNTs/CTS/GCE.

Furthermore, when dsDNA/MWNTs/CTS/GCE was scanned in the buffer solution containing 7.5×10^{-4} M 6-MP, the oxidation peak current of guanine in dsDNA decreased and the characteristic oxidation peak of adenine disappeared. These observations implied that the damage to dsDNA induced by 6-MP was severe, especially to adenine. This was because that with the addition of 6-MP, 6-MP and dsDNA interacted, and 6-MP embedded into dsDNA double helix structure, causing

serious damage to the dsDNA. As a result, the oxidation-reduction reactions of bases were hindered and the oxidized guanine, especially for the oxidized adenine, decreased, thus, the oxidation peak current declined.

3.7 Influence of the ionic strength on the interaction

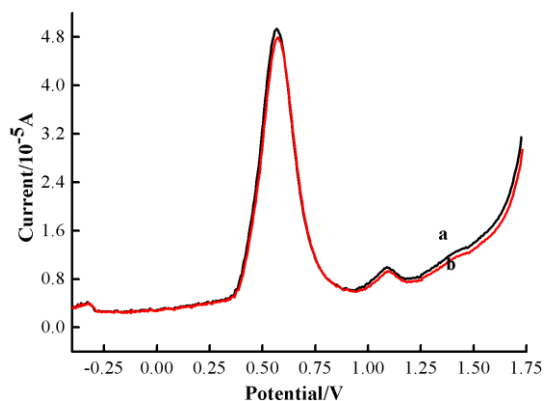


Fig. 9. The influence of Na^+ on DPV of the dsDNA/MWNTs/CTS/GCE interact with 6.0×10^{-3} M 6-MP in phosphate buffer (pH 5.0, 0.1 M). (a) without NaCl and (b) with 0.03 M NaCl.

To further establish the mode of binding between 6-MP and DNA, the effect of ionic strength was detected by the addition of NaCl. There was almost no change in the DPV curves following addition of NaCl (Fig. 9). The 6-MP oxidation peak potential and the current at 0.6 V varied little, and the guanine oxidation peak at 1.1 V was not changed much, either, which indicated that the interaction between 6-MP and DNA was intercalation rather than the electrostatic interaction^{33, 34}. This result is consistent with the conclusion above.

3.8 Interaction between dsDNA and 6-MP

3.8.1 Effect of pH on the interactions

The equilibrium potential can reflect the redox ability of substances and indicate the possibility for an electrochemical reaction. If protons and electrons are involved in the reaction, the electrode potential will vary as the pH of the solution changes.

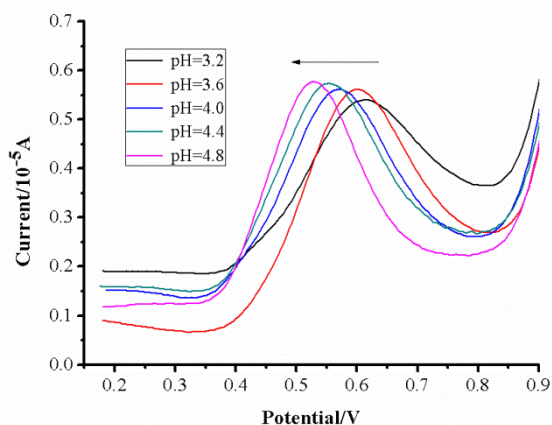


Fig. 10. The DPV curves of dsDNA/MWNTs/CTS/GCE in phosphate buffer (pH 5.0, 0.1 M) containing 7.5×10^{-4} M 6-MP at different pH values.

Fig. 10 shows that the oxidation potential of 6-MP gradually shifted toward the negative potential direction as the pH of the solution increased from 3.2 to 4.8. The curve was plotted, and the pH of the buffer solution and the potential of the 6-MP oxidation peak were adopted as the abscissa and ordinate, respectively. Subsequently, a linear fit for the relationship between the peak electric potential (E) and the pH value was established, and the fitting equation was as follows:

$$E/V = 0.799 - 0.0562\text{pH}, \quad (R^2 = 0.9685) \quad (5)$$

According to Ref.³⁵, if the slope of the linear equation is close to 59 mV/pH of the ideal state (25 °C), the same number of protons and electrons are involved in the interactions between small molecules and dsDNA during the electrochemical oxidation process on the modified electrode. As indicated by the slope of the linear equation (5), the slope value was 56.2 mV/pH, which suggested that there was an equal ratio of protons and electrons involved in the redox reaction of 6-MP according to Nernst equation.

3.8.2 Effects of scan rate on the interactions

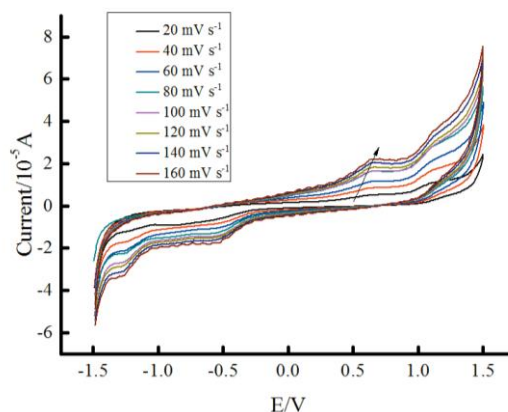


Fig. 11. The CV curves of dsDNA/MWNTs/CTS/GCE in phosphate buffer (pH 5.0, 0.1 M) containing 7.5×10^{-4} M 6-MP at different sweep speeds.

As shown in Fig. 11, the oxidation peak current steadily increased as the scan rate increased from 20 to 160 mV/s. The curve for the relationship between the scan rate and the oxidation peak current for 6-MP was plotted. After performing a linear fit, the equation between the oxidation current intensity (i) of 6-MP and the scan rate (v) was obtained as follows:

$$i/(\mu\text{A}) = 0.11v/(\text{mV/s}) + 1.29, \quad (R^2 = 0.990) \quad (6)$$

According to Ref.³⁶, if the relationship between the peak current and scan rate is linear, the electrochemical reaction is adsorption controlled, and if the relationship between the peak current and the square of the scan rate is linear, the reaction is diffusion controlled. The results of Eq. (6) indicated a linear relationship between the oxidation current of 6-MP and the scan rate, and moreover, there was a large shift in the redox peak potential as the scan rate increased, which suggested that the electrode reaction was an irreversible

process³⁷. Thus, the electrochemical oxidation of 6-MP on dsDNA/MWNTs/CTS/GCE was an irreversible process that was controlled by adsorption.

For a completely irreversible electrochemical oxidation process controlled by adsorption, the oxidation peak potential can be defined as following equation:

$$E_p = E^0 + (RT/\alpha nF) \ln(RT k_s/\alpha nF) + (RT/\alpha nF) \ln v \quad (7)$$

Based on the above data (Fig. 11), the linear equation between the oxidation peak potential of 6-MP and $\ln v$ was fitted:

$$E_p/V = 0.0388 \ln v/(mV s^{-1}) + 0.4105 \quad (R^2 = 0.9642) \quad (8)$$

Combining equation (7) and (8), it was calculated that $\alpha n = 0.44$. Because $0.3 < \alpha < 0.7$ during irreversible process, therefore $\alpha = 0.44$, $n = 1$.

Based on the results of Figure 10, we determined that a single proton and a single electron transfer were involved in the electrochemical oxidation process of 6-MP and DNA.

4. Conclusions

The modifications of MWNTs/CTS have significantly improved the electro-catalysis performance and biocompatibility of GCE. After modified, the active area of the MWNTs/CTS/GCE and its oxidation peak current of $K_3[Fe(CN)_6]$ significantly increased. The damage to adenine caused by 6-MP was more severe than to guanine. The primary mode of binding between 6-MP and dsDNA was demonstrated to be intercalation. The electrochemical oxidation of 6-MP on the dsDNA/PANI/CTS/GCE was irreversible and controlled by the adsorption process, which was accompanied by the transfer of a single electron coupled with a single proton during the process.

5. Acknowledgements

This work was supported by the National Natural Science Foundation of China (No. 21277098).

6. References

- C. Cai, X. Chen and H. Gong, *Spectrochimica Acta Part A: Molecular and Biomolecular Spectroscopy*, 2009, **72**, 46-49.
- R. Palchaudhuri and P. J. Hergenrother, *Current opinion in biotechnology*, 2007, **18**, 497-503.
- S. Takeuchi, T. Matsuda, S. Kobayashi, T. Takahashi and H. Kojima, *Toxicology and applied pharmacology*, 2006, **217**, 235-244.
- A. K. Williams, S. C. Dasilva, A. Bhatta, B. Rawal, M. Liu and E. A. Korobkova, *Analytical biochemistry*, 2012, **422**, 66-73.
- H.-Y. Shen, H.-M. Zheng, N. Zhu, Y.-Q. Liu, J. Gao and J. Li, *Int. J. Electrochem. Sci*, 2010, **5**, 1587-1596.
- L. Wang, H. Xiong, X. Zhang and S. Wang, *Electrochemistry Communications*, 2009, **11**, 2129-2132.
- N. Li, Y. Ma, C. Yang, L. Guo and X. Yang, *Biophysical chemistry*, 2005, **116**, 199-205.
- M. Tarun, B. Bajrami and J. F. Rusling, *Analytical chemistry*, 2006, **78**, 624-627.
- V. Viswesh, K. Gates and D. Sun, *Chemical research in toxicology*, 2009, **23**, 99-107.
- A. Asan and I. Isildak, *Journal of Chromatography A*, 2003, **988**, 145-149.
- S. Dong, L. Chi, Z. Yang, P. He, Q. Wang and Y. Fang, *Journal of separation science*, 2009, **32**, 3232-3238.
- A. A. Ensafi, M. Amini and B. Rezaei, *Sensors and Actuators B: Chemical*, 2013, **177**, 862-870.
- F. Gugliesi, M. Bawadekar, M. De Andrea, V. Dell'Oste, V. Caneparo, A. Tincani, M. Gariglio and S. Landolfo, *PLoS one*, 2013, **8**, e63045.
- Y. Wang, H. Xiong, X. Zhang and S. Wang, *Sensors and Actuators B: Chemical*, 2012, **161**, 274-278.
- D. Zhang, Y. Cui, H. Shen, L. Xing, J. Cui, J. Wang and X. Zhang, *PLoS one*, 2013, **8**, e65044.
- M. F. Barroso, N. De-los-Santos-Alvarez, M. J. Lobo-Castañón, A. J. Miranda-Ordieres, C. Delerue-Matos, M. B. P. P. Oliveira and P. Tuñón-Blanco, *Biosensors and Bioelectronics*, 2011, **26**, 2396-2401.
- A. A. Ensafi, B. Rezaei, M. Amini and E. Heydari-Bafrooei, *Talanta*, 2012, **88**, 244-251.
- T. Liao, Y. Wang, X. Zhou, Y. Zhang, X. Liu, J. Du, X. Li and X. Lu, *Colloids and Surfaces B: Biointerfaces*, 2010, **76**, 334-339.
- A. P. Schuch, J. C. Lago, T. Yagura and C. F. M. Menck, *PLoS one*, 2012, **7**, e40344.
- M.-Y. Wei, L.-H. Guo and P. Famouri, *Microchimica Acta*, 2011, **172**, 247-260.
- Y. Zheng, C. Yang, W. Pu and J. Zhang, *Microchimica Acta*, 2009, **166**, 21-26.
- P.-Y. Chen, R. Vittal, P.-C. Nien and K.-C. Ho, *Biosensors and Bioelectronics*, 2009, **24**, 3504-3509.
- Y. Wu, *Food chemistry*, 2010, **121**, 580-584.
- G.-S. Lai, H.-L. Zhang and D.-Y. Han, *Microchimica Acta*, 2008, **160**, 233-239.
- D. J. Abernethy, E. V. Kleymenova, J. Rose, L. Recio and B. Faiola, *Toxicological Sciences*, 2004, **79**, 82-89.
- L. Luo, L. Jiang, C. Geng, J. Cao and L. Zhong, *Chemico-biological interactions*, 2008, **173**, 1-8.
- R. Zhang, J. Zhu, G. Zhao and H. Chen, *CHEMICAL JOURNAL OF CHINESE UNIVERSITIES-CHINESE*, 1998, **19**, 1363-1368.
- N.-L. REN, B.-Z. ZENG, W.-M. Zhang and X.-Y. Zhou, *Journal of Analytical Science*, 1993, **3**, 007.
- R. N. Adams, 1969.
- G. Aydoğdu, G. Günendi, D. K. Zeybek, B. Zeybek and Ş. Pekyardımcı, *Sensors and Actuators B: Chemical*, 2014, **197**, 211-219.
- K.-J. Huang, D.-J. Niu, J.-Y. Sun, C.-H. Han, Z.-W. Wu, Y.-L. Li and X.-Q. Xiong, *Colloids and Surfaces B: Biointerfaces*, 2011, **82**, 543-549.
- X. Tian, Y. Song, H. Dong and B. Ye,

- Bioelectrochemistry*, 2008, **73**, 18-22.
33. A. Erdem, K. Kerman, B. Meric, U. S. Akarca and M. Ozsoz, *Analytica Chimica Acta*, 2000, **422**, 139-149.
34. W. Tang, M. Zhang, W. Li and X. Zeng, *Talanta*, 2014, **127**, 262-268.
35. T. Łuczak, *Electrochimica Acta*, 2008, **53**, 5725-5731.
36. Y. Wu and S. Hu, *Bioelectrochemistry*, 2007, **70**, 335-341.
37. L. Wei, Master, Huazhong University of Science and Technology, 2012.

Figure captions

Fig. 1. Raman spectrum of MWNTs.

Fig. 2. The CV curves of different modified electrodes in a 0.2 M KCl solution containing

5×10^{-3} M $K_3[Fe(CN)_6]$.

Fig. 3. The EIS curves of different modified electrodes in a 0.1 M KCl solution containing 5×10^{-3} M $K_3[Fe(CN)_6]/K_4[Fe(CN)_6]$.

Fig. 4. The CV curves of the electrodes modified with different concentrations of MWNTs in a 0.2 M KCl solution containing 5×10^{-3} M $K_3[Fe(CN)_6]$.

Fig. 5. The EIS curves of the electrodes modified with different concentrations of MWNTs in a 0.1 M KCl solution containing 5×10^{-3} M $K_3[Fe(CN)_6]/K_4[Fe(CN)_6]$.

Fig. 6. The $Q \sim t^{1/2}$ curves of different modified electrodes in a 1 M KCl solution containing 1×10^{-4} M $K_3[Fe(CN)_6]$.

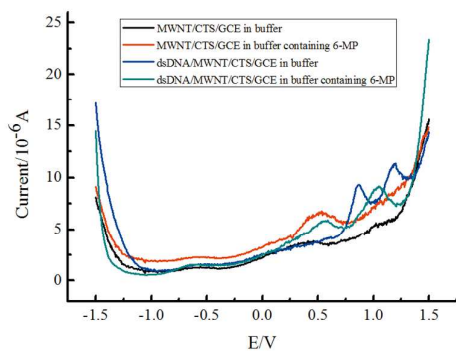
Fig. 7. The DPV curves of dsDNA on different modified electrodes in phosphate buffer (pH 5.0, 0.1 M).

Fig. 8. The DPV curves of MWNTs/CTS/GCE and dsDNA/MWNTs/CTS/GCE in phosphate buffer (pH 5.0, 0.1 M) and phosphate buffer (pH 5.0, 0.1 M) containing 7.5×10^{-4} M 6-MP, respectively.

Fig. 9. The influence of Na^+ on DPV of the dsDNA/MWNTs/CTS/GCE interact with 6.0×10^{-3} 6-MP in phosphate buffer (pH 5.0, 0.1 M). (a) without NaCl and (b) with 0.03 M NaCl.

Fig. 10. The DPV curves of dsDNA/MWNTs/CTS/GCE in phosphate buffer (pH 5.0, 0.1 M) containing 7.5×10^{-4} M 6-MP at different pH values.

Fig. 11. The CV curves of dsDNA/MWNTs/CTS/GCE in phosphate buffer (pH 5.0, 0.1 M) containing 7.5×10^{-4} M 6-MP at different sweep speeds.



Clear damage to dsDNA caused by 6-MP was observed. The damage to adenine was more severe than to guanine.